第29卷 第10期 半导体学报 Vol.29 No.10
2008年10月 JOURNAL OF SEMICONDUCTORS Oct.,2008

Impact of Lattice Volume on the Band Gap Broadening of Isovalent S-Doped $CuInSe_2$ *

Chen Xiang[1], Zhao Yujun[1,†], Yao Ruohe[1], and He Julong[2]

(1 *Department of Physics, South China University of Technology, Guangzhou 510640, China*)

(2 *Key Laboratory of Metastable Materials Science and Technology, Yanshan University, Qinhuangdao 066004, China*)

Abstract: The electronic structure of pure and S-doped chalcopyrite $CuInSe_2$ is investigated using a first-principles pseudopotential method in the generalized gradient approximation. The calculation indicates that the band gap of $CuInSe_2$ broadens as S-doping concentration increases. We find that the decreased lattice volume due to isovalent S-doping in $CuInSe_2$ has a significant impact on the band gap broadening phenomena. This physical insight is further discussed with the study of the electronic structure and bond length changes.

Key words: first-principles calculation; $CuInSe_2$; band gap broadening

PACC: 3000; 3120A; 7115A

CLC number: O471.5 **Document code**: A **Article ID**: 0253-4177(2008)10-1883-06

1 Introduction

Solar cells based on copper ternary chalcogenide compounds and alloys have emerged over the last 20 years as a promising solution to the high-cost problem of solar cells. The ternary Ⅰ-Ⅲ-$Ⅵ_2$ compound $CuInSe_2$(CIS) is a member of the chalcopyrite semiconductor family. CIS has been regarded as a very promising material for thin film solar cells due to its strong absorption of sunlight[1,2]. However, the band gap of CIS (1.04eV) deviates by ~0.5eV from the optimal band gap of 1.5eV for single junction solar cells[3]. According to experiments in Refs.[4,5], CIS can be isovalent doped by Ga or S to increase its band gap and improve its conversion efficiency. In fact, CIS and related $Cu(In,Ga)(S,Se)_2$ material have been extensively studied experimentally and theoretically[6~9]. Using thin film technology, the conversion efficiencies of CIS and related $Cu(In,Ga)(S,Se)_2$ material have been improved up to 22.5%[10~13].

In this paper, we systematically study the electronic structure of pure and S-doped chalcopyrite CIS over a range of concentrations using a first-principles pseudopotential method within the generalized gradient approximation. The band broadening phenomena are investigated according to the geometrical and chemical contributions due to S doping.

2 Computation

As shown in the crystal structure (Fig.1), CIS belongs to the chalcopyrite crystal structure of type ABC_2. The 16-atom supercell employed in our calculation consists of two primitive unit cells. The space group of CIS, which belongs to the chalcopyrite crystal structure, is $I\bar{4}2D$. The experimental lattice constants of CIS are: $a = 0.5796$nm; $c = 1.1614$nm[14]. $CuIn(S_xSe_{1-x})_2$ can be obtained through partially substituting the element Se by S at the C lattice sites of ABC_2.

The density functional theory (DFT)[15] based first-principles calculations are performed with the

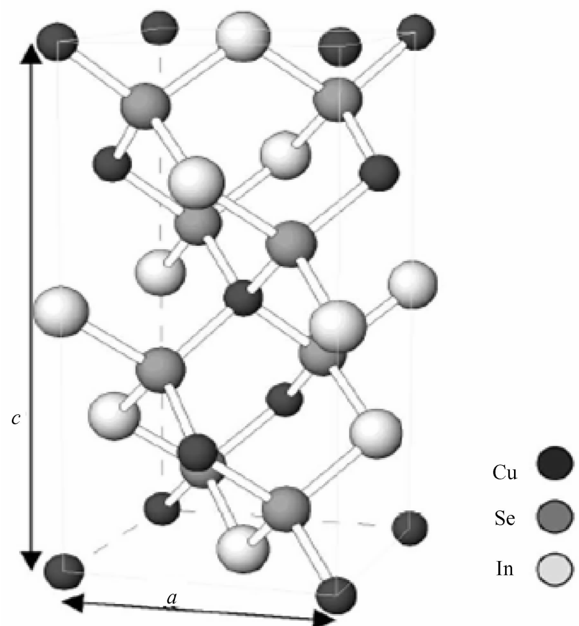

Fig.1 Chalcopyrite structure for $CuInSe_2$ crystal

* Project supported by the High Performance Computer Center of South China University of Technology

† Corresponding author. Email: zhaoyj@scut.edu.cn

Received 3 March 2008, revised manuscript received 21 May 2008

©2008 Chinese Institute of Electronics

Table 1 Lattice parameters of $CuInSe_2$ from experiment and theory

	Theory		Experiment
	This work	Ref.[23]	Ref.[14]
a/nm	0.5839	0.5733	0.5796
c/nm	1.1738	1.1524	1.1614
$c/2a$	1.005	1.005	1.002

Cambridge serial total energy package CASTEP[16]. The Norm-conserving pseudopotential[17] and generalized gradient approximation (GGA-PW91)[18] are employed in our calculations①. Pseudo-atomic calculations are performed for Cu-$3d^{10}4s^1$, In-$5s^2 5p^1$, Se-$4s^2 4p^4$, and S-$3s^2 3p^4$. The plane-wave basis set cutoff is chosen to be 660eV. The Monkhorst-Pack method[19] with a $4 \times 4 \times 2$ special k-points mesh is employed for the reciprocal space integration over the Brillouin zone. As a convergence test, we find the band gap of CIS changes by only 0.001eV when the k-mesh is increased to $6 \times 6 \times 4$. The Broyden-Fletcher-Goldfarb-Shanno (BFGS) minimization scheme[20] is used in the geometry optimization, while the pulay[21] method is employed for electronic minimization. The convergent criterion of the total energy is set to be 2.0×10^{-6}eV/atom.

3 Results and discussion

3.1 Pure $CuInSe_2$

Comparisons of our present results with earlier calculations and an experiment are given in Table 1. The computed lattice constants a and c in this work are overestimated by about 1% compared with the experimental results[14], while their equilibrium volumes are within 3% error. In Ref.[23], the lattice constants were calculated by SIESTA, where the atom-centered localized numerical basis along with norm-conserving pseudopotentials is employed. The results were underestimated by 1%. The $c/2a$ ratio remains very close to 1.0 in $CuInSe_2$, similar to the earlier experimental and theoretical results.

The calculated band structure is plotted in Fig.2 for CIS, in which the Fermi level is set to zero. The calculated band gap is 0.469eV, which is smaller than the experiment value because the correlation between the valence electrons is underestimated in the GGA[18]. The conduction band minimum (CBM) and valence band maximum (VBM) for $CuInSe_2$ are both located at the Γ point, indicating CIS as a direct-band-gap material.

To better understand the nature of the inter-atomic bonding, the electronic structure is examined. Figure 3 shows the total and atom-projected partial density of states (PDOS) of $CuInSe_2$. Gaussian smearing with the broadening parameter of 0.2eV is used for the plot of DOS. The lowest states from −14 to −11eV originate mainly from the Se4s state. The states ranging from −6.45 to −4.80eV are mainly composed of In5s and Se4p states. The states ranging from −4.80 to −2.50eV largely originate from the Se4p and Cu3d states with a small mixing of In5p. The VBM primarily originates from the Cu3d and Se4p states. The conduction bands (CBs) are composed of In5s, In5p, Se4s, and Se4p.

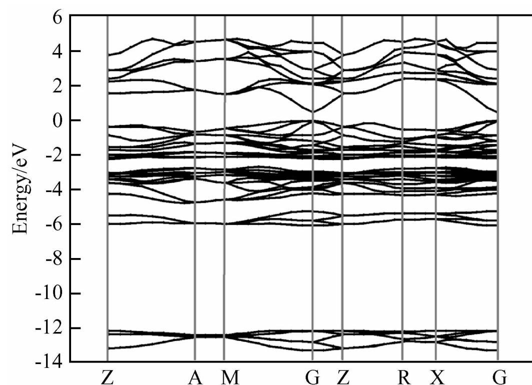

Fig.2 Calculated band structure for $CuInSe_2$ at the theoretical optimized lattice The Fermi level is set to zero.

3.2 $CuInSe_2$ with S-doping

$CuIn(S_x Se_{1-x})_2$ is obtained by partially substituting the element Se by S as uniformly distributed as possible. The lattice constants, electronic structure, and density of states are optimized with the corresponding concentration of S. The relation between the electronic structure and the concentration of S is studied by comparing the DOS in different concentrations of S.

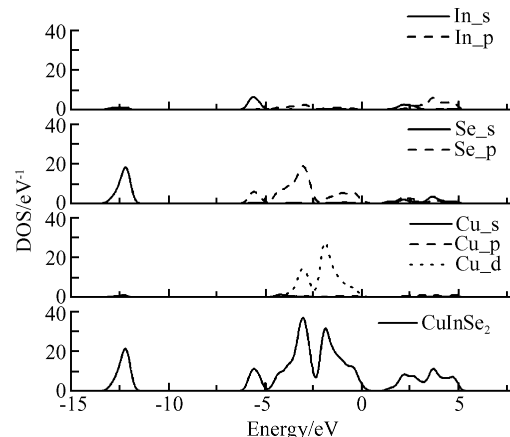

Fig.3 Calculated total DOS and atom-projected partial DOS of $CuInSe_2$ The Fermi level is set to zero.

① We test the calculation with the popularly used ultrasoft pseudopotential, but the LDA band gap underestimation is significant that no band gap is found in $CuInSe_2$. Thus norm-conserving pseudopotential is adopted in this work.

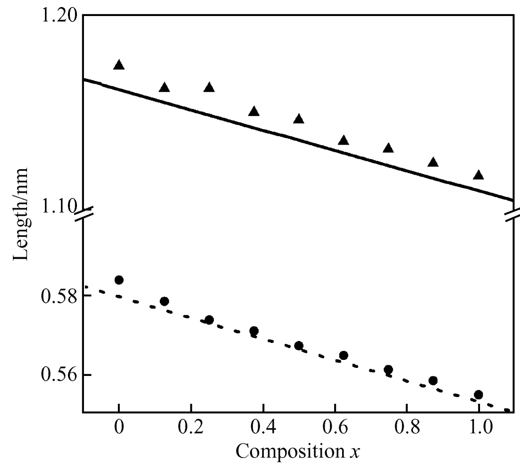

Fig. 4　Lattice constants of $CuIn(S_xSe_{1-x})_2$　The calculated c and a are denoted by ▲ and ●, respectively. The solid and dashed lines are fitted curves for experiment c and a, respectively[14].

3.2.1　Lattice constants

The lattice constants of $CuIn(S_xSe_{1-x})_2$ are optimized as done for $CuInSe_2$. The evolution of the a and c lattice constants as a function of the S concentration are shown in Fig. 4, which is in good agreement with Vegard's law[23]. The solid and dashed lines are linear fitted results for the experimental data[14]. The calculated lattice constants are overestimated by ~1%, which is within the typical DFT error. The ratio of $c/2a$ equates ~1.0 with the variation of S concentration. Because the covalence radius of S (0.102nm) is smaller than that of Se (0.117nm)[24], the lattice constants decrease as S concentration increases, as expected in $CuIn(S_xSe_{1-x})_2$.

3.2.2　Density of states

The total and atom-projected partial density of states of $CuIn(S_xSe_{1-x})_2$ ($x = 0.5$) are plotted in Fig. 5. The lowest states from −14 to −11eV originate mainly from Se4s and S3s. The states ranging from −6.45 to −2.50eV are mainly composed of In5s, Se4p, S3p, and Cu3d with a small mixing of In5p. The states whose range is from −2.50 to 0.0eV are mainly composed of Cu3d, Se4p, and S3p. The conduction bands originate mainly from In5s, In5p, Se4s, and Se4p with a small mixing of S3s and S3p.

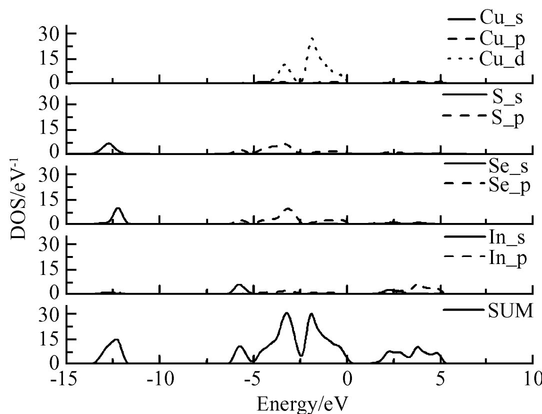

Fig. 5　Total DOS and atom-projected partial DOS of $CuIn(S_xSe_{1-x})_2$ ($x=0.5$)　The Fermi level is set to zero.

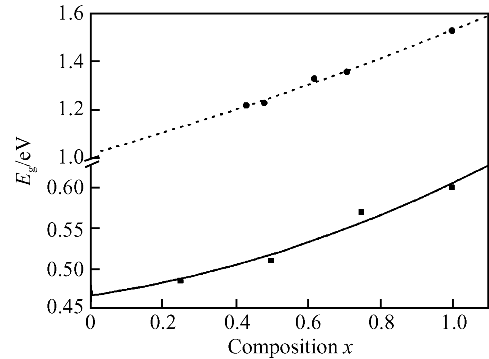

Fig. 6　Calculated and experimental[5] energy band gaps of $CuIn(S_xSe_{1-x})_2$ versus x　The calculated and experimental band gap are denoted by ■ and ●, respectively. The solid and dashed lines are the fitted curves for calculated and experimental band gaps, respectively.

3.2.3　Band gap broadening

The calculated and experimental band gaps of $CuIn(S_xSe_{1-x})_2$ versus the S concentration are given in Fig. 6. The calculation shows that the band gap of $CuIn(S_xSe_{1-x})_2$ broadens as the S-doping concentration increases, which agrees with the experiment result[5].

Figure 6 shows that the calculated band gaps are significantly smaller than the experiment values, due to the GGA error. However, the increasing trend of the band gap for $CuIn(S_xSe_{1-x})_2$ as x increases is consistent with that of the experiment.

It is easy to raise the question of how the lattice volume plays a role in the band gap broadening since the chemical properties of S and Se are very similar. We calculate the band gap of $CuInS_2$ [$E_g^*(CuInS_2)$] with the lattice constants of $CuInSe_2$, and the band gap of $CuInSe_2$ [$E_g^*(CuInSe_2)$] with the lattice constants of $CuInS_2$. The calculated band gaps and bond lengths are listed in Table 2. The table shows that the calculated energy band gap $E_g^*(CuInS_2)$ is 0.298eV, smaller than that of ideal $CuInSe_2$ (0.469eV); and $E_g^*(CuInSe_2)$ is 0.776eV, greater than that of ideal

Table 2　Energy band gap and bond length of $CuInSe_2$, $CuInSe_2^*$ (using the lattice constants of $CuInS_2$), $CuInS_2$, $CuInS_2^*$ (using the lattice constants of $CuInSe_2$) and CuInSeS

	E_g/eV	Cu-S/nm	Cu-Se/nm	In-S/nm	In-Se/nm
$CuInSe_2$	0.469	–	0.2430	–	0.2645
$CuInSe_2^*$	0.776	–	0.2289	–	0.2540
$CuInS_2$	0.600	0.2309	–	0.2516	–
$CuInS_2^*$	0.298	0.2451	–	0.2620	–
CuInSeS	0.510	0.2296	0.2431	0.2542	0.2616

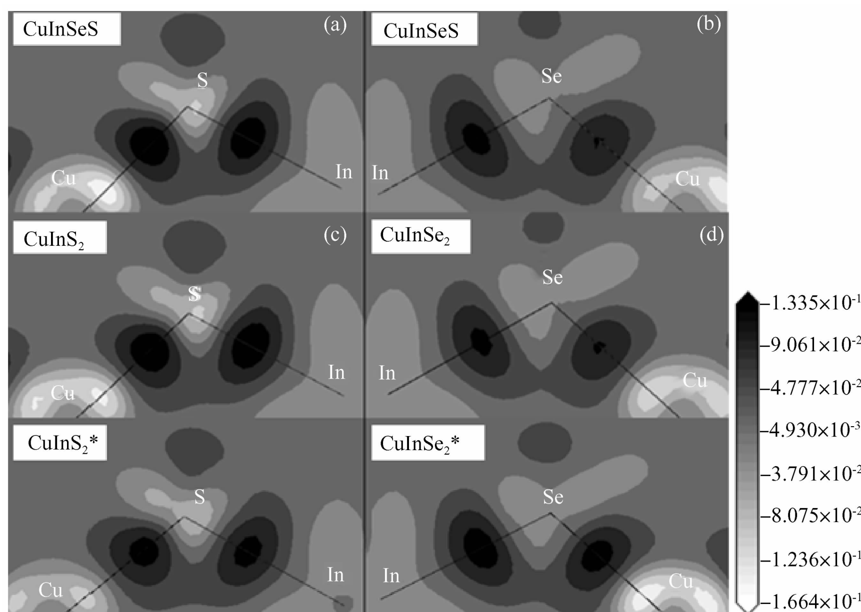

Fig.7 Electron density difference in the (110) plane for $CuIn(S_xSe_{1-x})_2$ at $x=0.5$ [(a) for plane containing S; (b) for plane containing Se], $CuInS_2$ (c) and $CuInSe_2$ (d), $CuInS_2$ (e) with $CuInSe_2$ lattice, and $CuInSe_2$ (f) with $CuInS_2$ lattice

$CuInS_2$ (0.600eV). The band gap change with respect to the lattice volume is consistent with the experimental observed pressure dependence of band gaps in $CuInSe_2$[25]. This indicates that the structure of the compound has the dominant influence on energy band gap broadening. The energy band gap broadens as the bond length decreases. The isovalent S substitution reduces the lattice volume of CIS, which pressures the Cu—Se—In bonds. The bond length of In—Se (In—S) in CuInSSe is shorter (longer) than that in ideal $CuInSe_2$ ($CuInS_2$), but longer (shorter) than that in $CuInSe_2^*$ ($CuInS_2^*$). However, the bond length of Cu—Se (Cu—S) in CuInSSe is longer (shorter) than that in both ideal $CuInSe_2$ ($CuInS_2$) and $CuInSe_2^*$ ($CuInS_2^*$). This may be due to the slightly greater difference between bond strength of Cu—Se and Cu—S in comparison with the difference between In—Se and In—S[①]. The bond length of Cu—S is shorter than that of Cu—Se in the equilibrium state, which means that the covalent bonds of Cu—S are stronger than those of Cu—Se, decreasing the lattice volume. So the band gap of $CuIn(S_xSe_{1-x})_2$ compound increases as the S concentration increases.

To further understand the effect of S-doping in $CuInSe_2$, the electron density difference, i.e., the difference between the alloy charge density and the superposition of atomic charge density, for $CuIn(S_xSe_{1-x})_2$ is plotted in Fig.7. Figures 7 (a) and 7(b) show the bonds of the Cu—S—In—Se—Cu in CuInSSe. Figures 7 (c) and 7(d) show the electron density difference for $CuInS_2$ and $CuInSe_2$, respectively, and Figures 7 (e) and 7(f) for $CuInS_2$ with lattice constants of $CuInSe_2$, and $CuInSe_2$ with lattice constants of $CuInS_2$, respectively. Comparing Figs. 7 (a) and 7 (b), the electron overlap of Cu—S—In bonds is higher than that of Cu—Se—In. The covalent bond of S—Cu and S—In are slightly stronger than that of Se—Cu and Se—In, respectively. The bond length of S—Cu (0.2296nm) and S—In (0.2542nm) are shorter than that of Se—Cu (0.2431nm) and Se—In (0.2616nm), correspondingly. When the lattice volume decreases, the covalent bond becomes stronger and the band gap increases. We find that when the lattice constants of $CuInSe_2$ and $CuInS_2$ are equal, the covalent bond of S—Cu is stronger than that of Se—Cu, but the band gap of $CuInSe_2$ is greater than that of $CuInS_2$. Figure 7 shows that the electron overlap on Cu—S and Cu—Se has no significant changes in CuInSSe compared with their ideal pure case. However, the electron overlap on In—Se increases slightly in CuInSSe with respect to ideal $CuInSe_2$ (c.f. Figs. 7 (b) and 7(d)), while the electron overlap on the In—S bond decreases slightly (c.f. Figs. 7(a) and 7(c)). This is in consistent with the corresponding bond length changes. As a result, the energy band gap of CuInSSe becomes greater than that of $CuInSe_2$ (although less than that of $CuInS_2$, as expected), and it will broaden as

① The calculated total energies for CuSe, CuS, InSe, and InS are −7.54, −8.28, −7.17, and −7.75eV per molecule unit, respectively. Here the P63/MMC, P63/MMC, R3M, and P21/N are adopted for CuSe, CuS, InSe, and InS compounds, respectively.

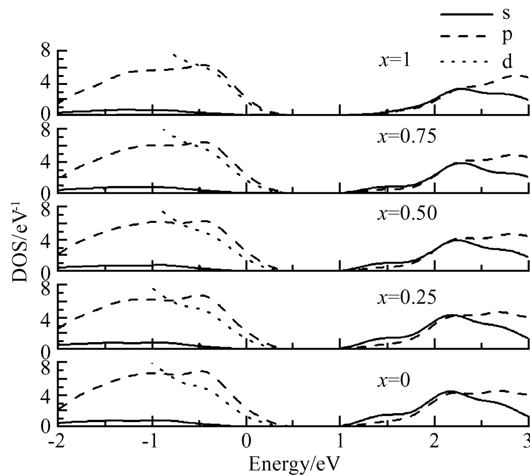

Fig. 8　PDOS of $CuIn(S_xSe_{1-x})_2$ near Fermi level for $x = 0$, 0.25, 0.50, 0.75 and 1　The Fermi level is set to zero.

the concentration of S increases.

According to the experiment, the VBM of CIS is 233meV higher than that of $CuInS_2$ and the CBM of CIS is 214meV lower than that of $CuInS_2$[26]. In order to understand the band gap changes from electronic structure, the PDOS of $CuIn(S_xSe_{1-x})_2$ near the Fermi level for $x = 0, 0.25, 0.50, 075$, and 1 are plotted in Fig. 8, respectively. The figure shows that when x increases, the hybridized Se4p and S3p states move closer to the Cu3d states, which means the p-d repulsion becomes stronger. But the energy of the p states increases from S to Se, so the anion p states decrease as x increases, which results in a higher VBM in $CuInSe_2$[27]. Figure 8 also shows that the s states in CBs near the Fermi level get closer to the p states as x increases. The position of CBM shifts upward when Se atoms are replaced by more S atoms due to the increasing s level energy from Se to S[27].

4　Summary

In summary, we have investigated the equilibrium crystal structure and electronic structure of $CuIn(S_xSe_{1-x})_2$ by first-principles calculations. The calculated lattice volume and trend of band gap for $CuIn(S_xSe_{1-x})_2$ are in excellent agreement with experimental observation. We demonstrate that the change of lattice volume plays a significant role in the band gap broadening of $CuIn(S_xSe_{1-x})_2$. We found that the In—Se bond length decreases in $CuIn(S_xSe_{1-x})_2$ while the bond length of Cu—Se has no remarkable changes. The CBM shifts upward due to the higher energy of S3s than that of the Se4s state, while the VBM shifts downward due to the higher energy of the Se4p state than that of the S3p state. As a result, the energy gap broadens in $CuIn(S_xSe_{1-x})_2$ as x increases.

References

[1] Rockett A, Birkmire R W. $CuInSe_2$ for photovoltaic applications. J Appl Phys, 1991, 70: R81
[2] Negami T, Nishitani M, Kohara N, et al. Real time composition monitoring methods in physical vapor deposition of Cu(In, Ga)-Se_2 thin films. Mater Res Soc Symp Proc, 1996, 426: 267
[3] Blankiewicz K, Bacewicz R, Trykozko R. Preparation and characterisation of CdTe thin films and CdTe based heterostructures. Warsaw University of Technology, 1992: 59
[4] Sheppard C J, Alberts V, Botha J R. Structural and optical characterization of single-phase $CuIn(Se,S)_2$ thin films deposited using a two-step process. Phys Status Solidi C, 2008, 5: 641
[5] Neff H, Lange P, Fearheiley M L, et al. Optical and electrochemical properties of $CuInSe_2$ and $CuInS_2$-$CuInSe_2$ alloys. Appl Phys Lett, 1985, 47: 1089
[6] Xu C M, Sun Y, Li F Y, et al. Composition-induced structural modifications in the quaternary $CuIn_{1-x}Ga_xSe_2$ thin films: bond properties versus Ga content. Chin Phys, 2007, 16: 788
[7] Zhao Y J, Persson C, Lany S, et al. Why can $CuInSe_2$ be readily equilibrium-doped n-type but the wider-gap $CuGaSe_2$ cannot. Appl Phys Lett, 2004, 85: 5860
[8] Walter T, Ruckh M, Velthaus K O, et al. Solar cells based on $CuIn(S,Se)_2$—a promising alternative. Proc 11th EC Photovoltaic Solar Energy Conf Montreux, 1992: 124
[9] Kondo K, Sano H, Sato K. Nozzle diameter effects on $CuInSe_2$ films grown by ionized cluster beam deposition. Thin Solid Films, 1998, 326: 83
[10] Zweibel K. Thin films: past, present, future. Progress in Photovoltaics, 1995, 3: 279
[11] Dimmler B, Schock H W. Scaling-up of CIS technology for thin-film solar modules. Progress in Photovoltatics: Research and Applications, 1996, 4: 425
[12] Guillemoles J F, Cowache P, Lusson A, et al. One step electrodeposition of $CuInSe_2$: improved structural, electronic, and photovoltaic properties by annealing under high selenium pressure. J Appl Phys, 1996, 79: 7293
[13] Guimard D, Bodereau N, Kurdi J, et al. Efficient CIGS solar cells prepared by electrodopisition. Proceeding of the 3rd Conference on Photovoltaic Energy Conversion, Osaka, Japan, 2003: 2P-P3-58
[14] Xiao Jianping, Xie Yi, Xiong Yujie, et al. A mild solvothermal route to chalcopyrite quaternary semiconductor $CuIn(Se_xS_{1-x})_2$ nanocrystallites. J Mater Chem, 2001, 11: 1417
[15] Hohenberg P, Kohn W. Inhomogeneous electron gas. Phys Rev B, 1964, 136: 864
[16] Segall M D, Lindan P L D, Probert M J, et al. First-principles simulation: ideas, illustrations and the CASTEP code. J Phys: Condensed Matter, 2002, 14: 2717
[17] Hamann D R, Schluter M, Chiang C. Norm-conserving pseudopotentials. Phys Rev Lett, 1979, 43: 1494
[18] Perdew J P, Chevary J A, Vosko S H, et al. Atoms, molecules, solids, and surfaces: applications of the generalized gradient approximation for exchange and correlation. Phys Rev B, 1992, 46: 6671
[19] Monkhorst H J, Pack J D. Special points for Brillouin-zone integrations. Phys Rev B, 1976, 13: 5188
[20] Pfrommer B G, Côté M, Louie S G, et al. Relaxation of crystals with the quasi-Newton method. J Comput Phys, 1997, 131: 233
[21] Kresse G, Furthmuller J. Efficient iterative schemes for ab initio total-energy calculations using a plane-wave basis set. Phys Rev B, 1996, 54: 11169
[22] Postnikov A V, Yakushev M V. Lattice dynamics and stability of $CuInSe_2$. Thin Solid Films, 2004, 451/452: 141
[23] Vegard L. The constitution of mixed crystals and the space occupied by atoms. Zeitschrift fuer Physik, 1921, 5: 17

[24] Miessler G L, Tarr D A. Inorganic chemistry. Prentice Hall, 2003: 45

[25] Choi I H, Yu P Y. Pressure dependence of band gaps in the quaternary semiconductors Cu(In, Ga)Se_2. Phys Status Solidi B, 1999, 211: 51

[26] Turcu M, Rau U. Compositional trends of defect energies, band alignments, and recombination mechanisms in the Cu(In, Ga)(Se, $S)_2$ alloy system. Thin Solid Films, 2003, 431/432: 158

[27] Wei S H, Zunger A. Band offsets and optical bowings of chalcopyrites and Zn-based II-VI alloys. J Appl Phys, 1995, 78: 3846

S 掺杂 $CuInSe_2$ 导致的体积变化对其禁带宽度的影响*

陈 翔[1] 赵宇军[1,†] 姚若河[1] 何巨龙[2]

(1 华南理工大学物理科学与技术学院，广州 510640)

(2 燕山大学材料科学与工程技术学院，秦皇岛 066004)

摘要： 运用第一性原理方法研究了 $CuInSe_2$ 和不同量的 S 掺杂 $CuInSe_2$ 所形成的化合物的电子结构. 理论计算表明，S 掺杂导致 $CuInSe_2$ 禁带宽度增大，且通过对其电子结构和键长的分析，发现因 S 掺杂浓度的增加而导致的 CuInSeS 化合物晶格体积减小对其禁带宽度的增加有重要的影响.

关键词： 第一性原理；$CuInSe_2$；禁带宽度

PACC： 3000；3120A；7115A

中图分类号： O471.5 **文献标识码：** A **文章编号：** 0253-4177(2008)10-1883-06

* 华南理工大学高性能计算中心资助项目

† 通信作者. Email: zhaoyj@scut.edu.cn

2008-03-03 收到，2008-05-21 定稿

©2008 中国电子学会